Supporting Information

Establishing Ultralow Activation Energies for Lithium Transport in Garnet Electrolytes

Federico M. Pesci,[1*] Antonio Bertei,[2] Rowena H. Brugge,[1] Steffen P. Emge,[3] A. K. Ola Hekselman,[1] Lauren E. Marbella,[4] Clare P. Grey[3] and Ainara Aguadero[1*]

1. Department of Materials, Imperial College London, London, SW7 2BP, UK

2. Department of Civil and Industrial Engineering, University of Pisa, 56122, Pisa, Italy

3. Department of Chemistry, University of Cambridge, Cambridge, CB2 1EW, UK

4. Department of Chemical Engineering, Columbia University, New York, NY 10027, USA

Structural Characterisation

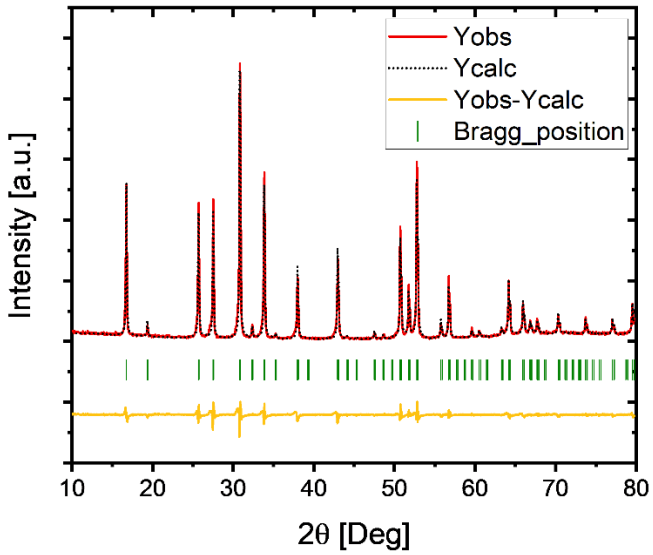

Figure S1: X-ray diffraction patterns (red line) and Rietveld refinement fittings (black dotted line) of $Li_{6.55}Ga_{0.15}La_3Zr_2O_{12}$ *indicating a cubic crystal structure with the* $Ia\bar{3}d$ *space group.*

Kramers-Kronig Validity Test

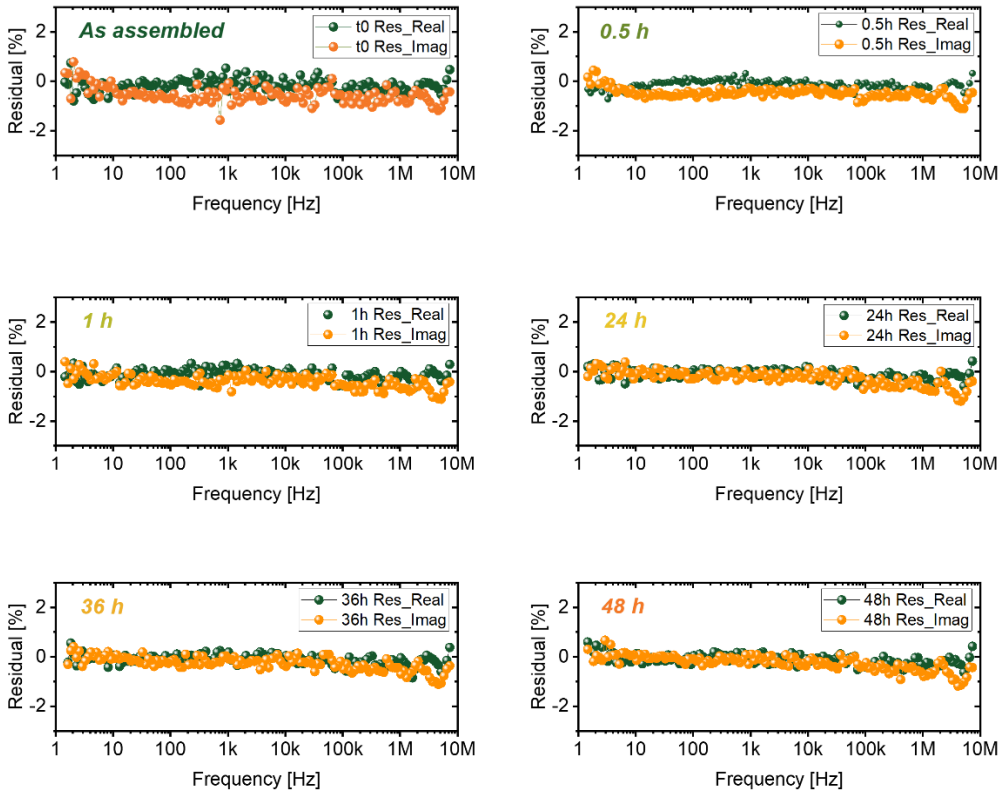

Figure S2: Kramers-Kronig residuals analysis for the EIS spectra recorded for a Ga-LLZO pellet at different times following cell assembly.

DRT Analysis of Variable Temperature EIS Spectra

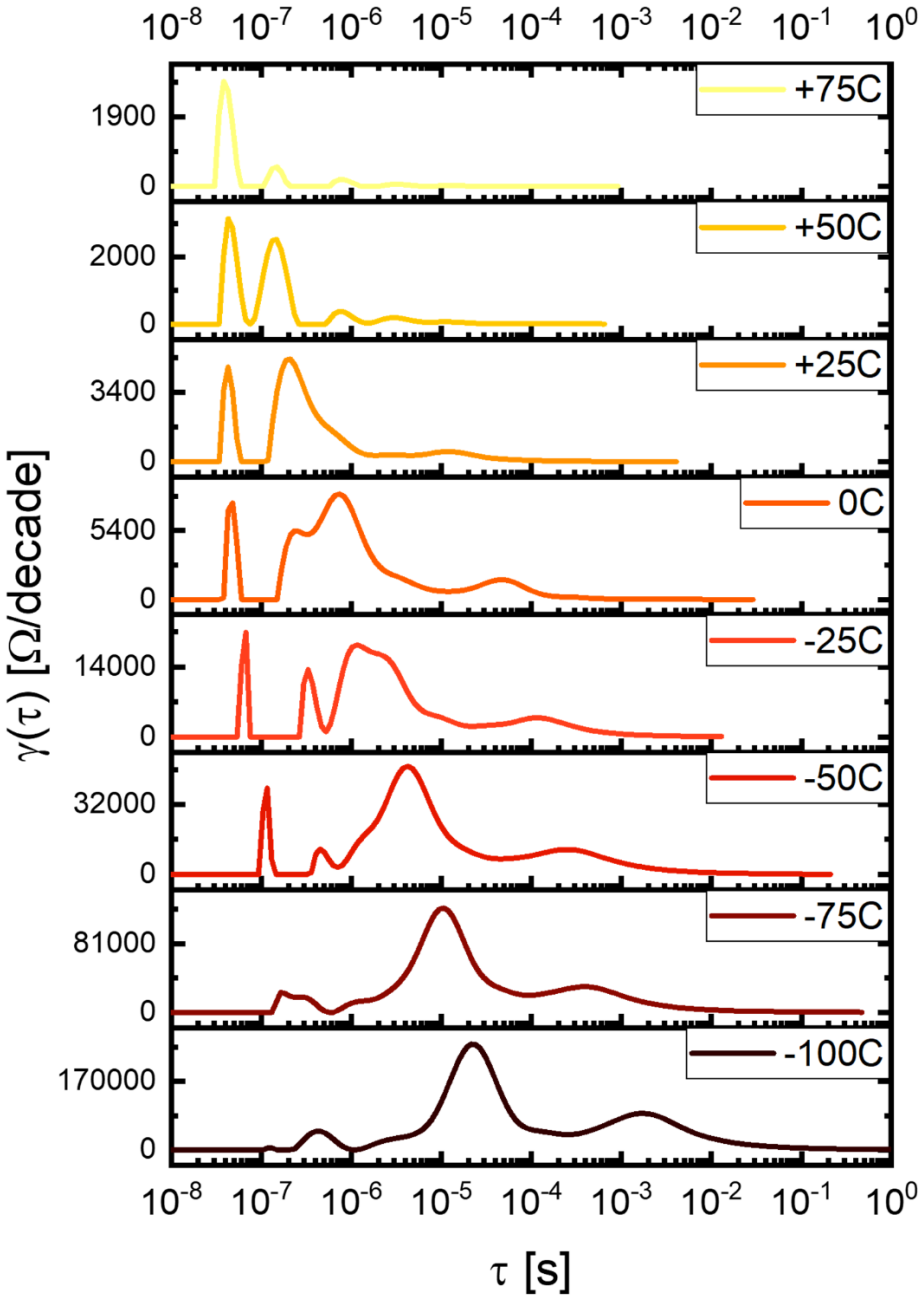

Figure S3: DRT analysis carried out on a symmetric cell of Ga-doped LLZO at different temperatures between -100°C to +75°C.

Fitting Results Calculated from Variable Temperature EIS Spectra

Table S1: EIS fitting results calculated from the EIS spectra recorded in the T range -100 °C to +75°C for a Li/LLZO/Li symmetrical cell. The numbers in brackets indicate the % error calculated from the fitting of the spectra.

	R_b (Ω cm)	C_b (F)	R_{gb} (Ω cm)	C_{gb} (F)	R_{int} (Ω cm^2)	C_{int} (F)
-100°C	32100 (2%)	1.28×10^{-11} (2%)	561673 (1%)	3.97×10^{-11} (4%)	18570 (2%)	2.35×10^{-8} (7%)
-75°C	16017 (2%)	1.41×10^{-11} (2%)	268492 (1%)	3.85×10^{-11} (4%)	5824 (3%)	1.79×10^{-8} (11%)
-50°C	7090 (1%)	1.54×10^{-11} (1%)	114126 (1%)	3.65×10^{-11} (1%)	2324 (2%)	2.82×10^{-8} (6%)
-25°C	2785 (1%)	1.74×10^{-11} (2%)	48997 (0.5%)	3.34×10^{-11} (2%)	593 (2%)	5.16×10^{-8} (5%)
0°C	1621 (3%)	1.49×10^{-11} (14%)	21144 (0.5%)	3.03×10^{-11} (4%)	165 (3%)	7.15×10^{-8} (16%)
+25°C	1167 (2%)	1.83×10^{-11} (2%)	8190 (0.7%)	3.04×10^{-11} (4%)	65 (4%)	4.68×10^{-8} (8%)
+50°C	816 (1%)	1.65×10^{-11} (0.4%)	3017 (0.3%)	3.49×10^{-11} (0.7%)	29 (2%)	1.88×10^{-8} (5%)
+75°C	535 (1%)	1.74×10^{-11} (0.6%)	803 (1%)	7.79×10^{-11} (2%)	18 (3%)	$6.47z10^{-9}$ (7%)

Activation Energy of Interfacial Processes

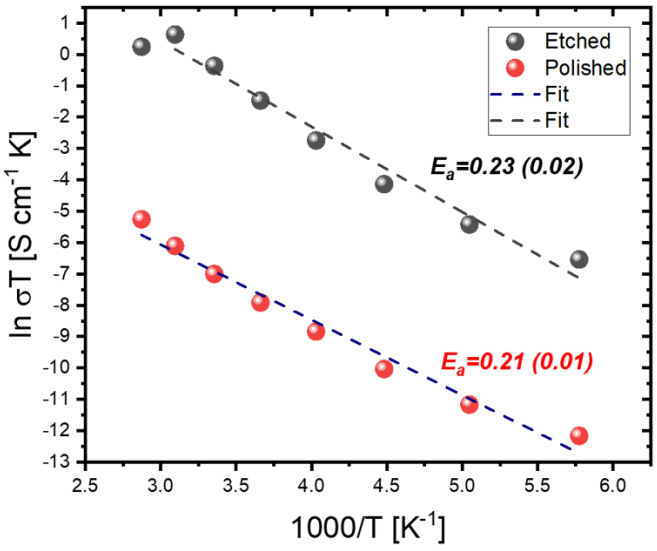

Figure S4: Arrhenius-type plot for E_a calculations of interfacial processes in Ga-LLZO polished and thermally etched samples, showing similar values for both cases.

Spin-lattice Relaxation, T_1, NMR for LLZO Powders

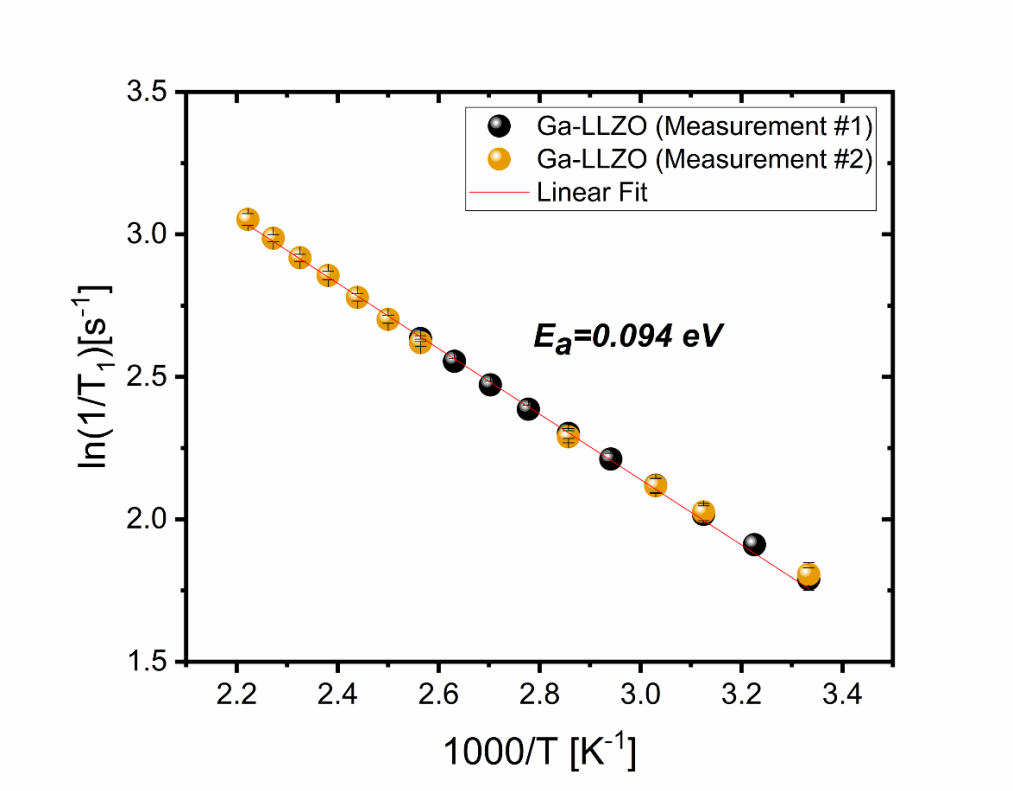

Figure S5: Variable temperature T1 data for Ga-doped LLZO used to extract activation energies, resulting in 0.094 eV. Measurement #1 was performed for ascending temperatures, while Measurement #2 was performed for the same sample and set-up but descending temperatures. The overlap shows a sufficient equilibration time between each experiment and stable sample behavior.

PFG-NMR analysis

The root mean square displacement (RMSD) $\sqrt{\langle x^2 \rangle}$ can be calculated from the diffusion coefficient, *D*, and the diffusion time, Δ:[1] (Equation S1)

$$\sqrt{\langle x^2 \rangle} = \sqrt{2D\Delta} \qquad \text{Equation S1}$$

In this case a factor of 2 is used since the PFG experiment measures transport only in one direction (along the z-Gradient).[2]

Table S2: Overview of PFG-NMR analysis of Al/Ga-LLZO samples at different temperatures.

	T/K	$D/10^{-13}$ [m²/s]	Δ/ms	$\sqrt{\langle x^2 \rangle}/\mu m$
Ga-LLZO	453	45.58	60	0.74
	433	38.21	60	0.68
	413	31.42	60	0.61
Al-LLZO	453	4.939	150	0.39
	433	3.446	150	0.32
	413	2.235	150	0.26
	393	1.39	150	0.20

Given that the RMSD value in Table S2 is much lower than the grain size as seen in Figure 1 it is safe to assume that we are probing the bulk diffusion with only limited grain boundary contributions.

Arrhenius Plot for Al-doped LLZO

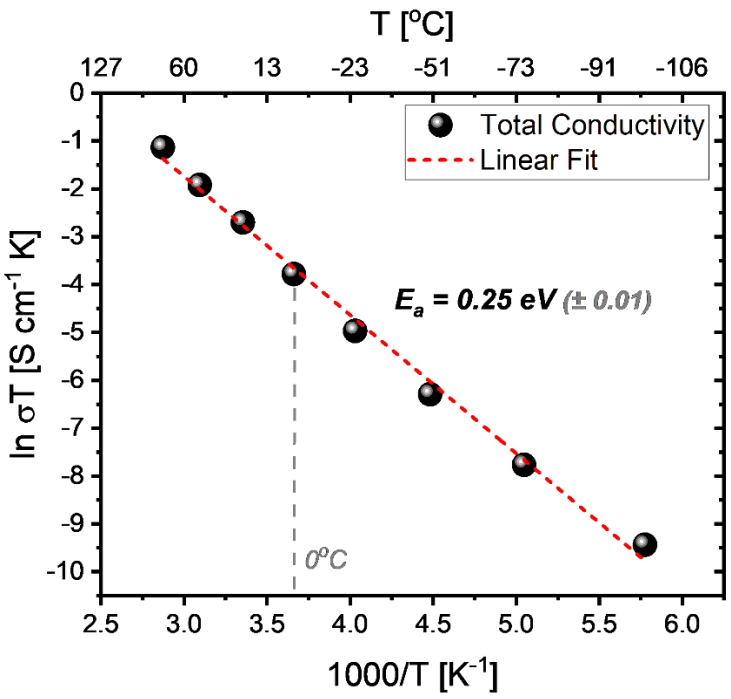

Figure S6: Arrhenius-type plot for E_a calculations of an Al-doped LLZO pellet, showing a constant E_a across the whole measured T range.

Activation Energies from Different Sets of Samples

Table S3: Values of activation energy of several LLZO samples calculated from variable temperature EIS measurements

	Bulk	*GB above 0 °C*	*GB below 0 °C*	*Total above 0 °C*	*Total below 0 °C*
Sample 1	0.15 eV	0.38 eV	0.14 eV	0.33 eV	0.14 eV
Sample 2 (Au)	0.14 eV	0.30 eV	0.12 eV	0.30 eV	0.12 eV
Sample 3	0.10 eV	0.46 eV	0.13 eV	0.23 eV	0.12 eV
Sample 4 (Au)	0.14 eV	0.36 eV	0.14 eV	0.25 eV	0.14 eV
Sample 5	0.11 eV	0.40 eV	0.10 eV	0.22 eV	0.10 eV

ToF-SIMS maps

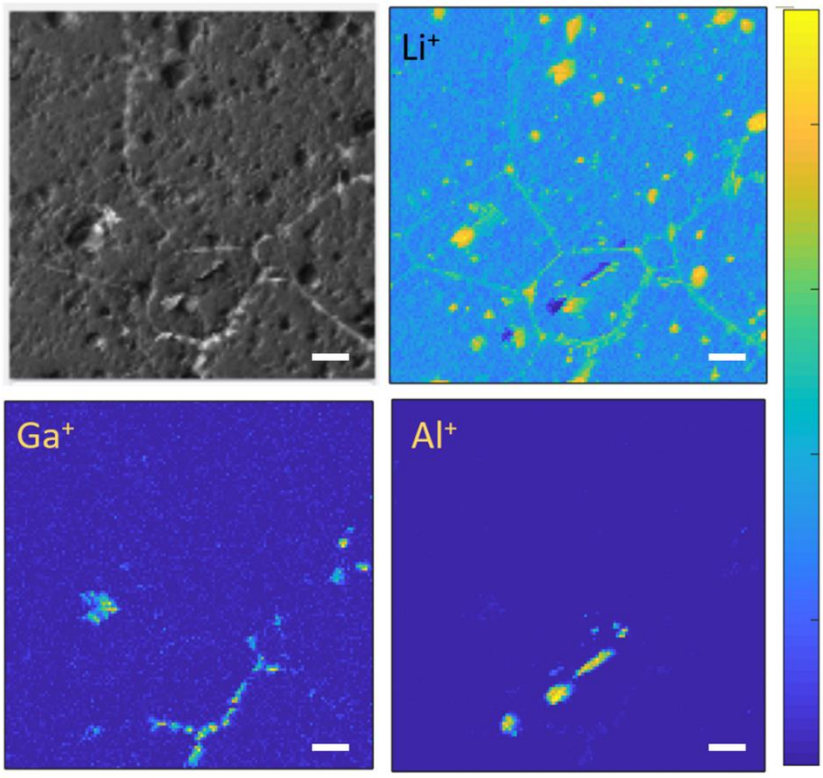

Figure S7: ToF-SIMS positive secondary ion images and elemental maps for Li^+, Al^+ and Ga^+, highlighting the segregation of dopants at the grain boundaries (scale bars: 20 μm).

Bibliography

(1) von Smoluchowski, M. Zur Kinetischen Theorie Der Brownschen Molekularbewegung Und Der Suspensionen. *Ann. Phys.* **1906**, *326* (14), 756–780. https://doi.org/10.1002/andp.19063261405.

(2) Engelke, S.; Marbella, L. E.; Trease, N. M.; De Volder, M.; Grey, C. P. Three-Dimensional Pulsed Field Gradient NMR Measurements of Self-Diffusion in Anisotropic Materials for Energy Storage Applications. *Phys. Chem. Chem. Phys.* **2019**, *21* (8), 4538–4546. https://doi.org/10.1039/c8cp07776b.